Volume 10
Number 6
14 February 2022
Pages 2583–3236

Journal of Materials Chemistry A

Materials for energy and sustainability

rsc.li/materials-a

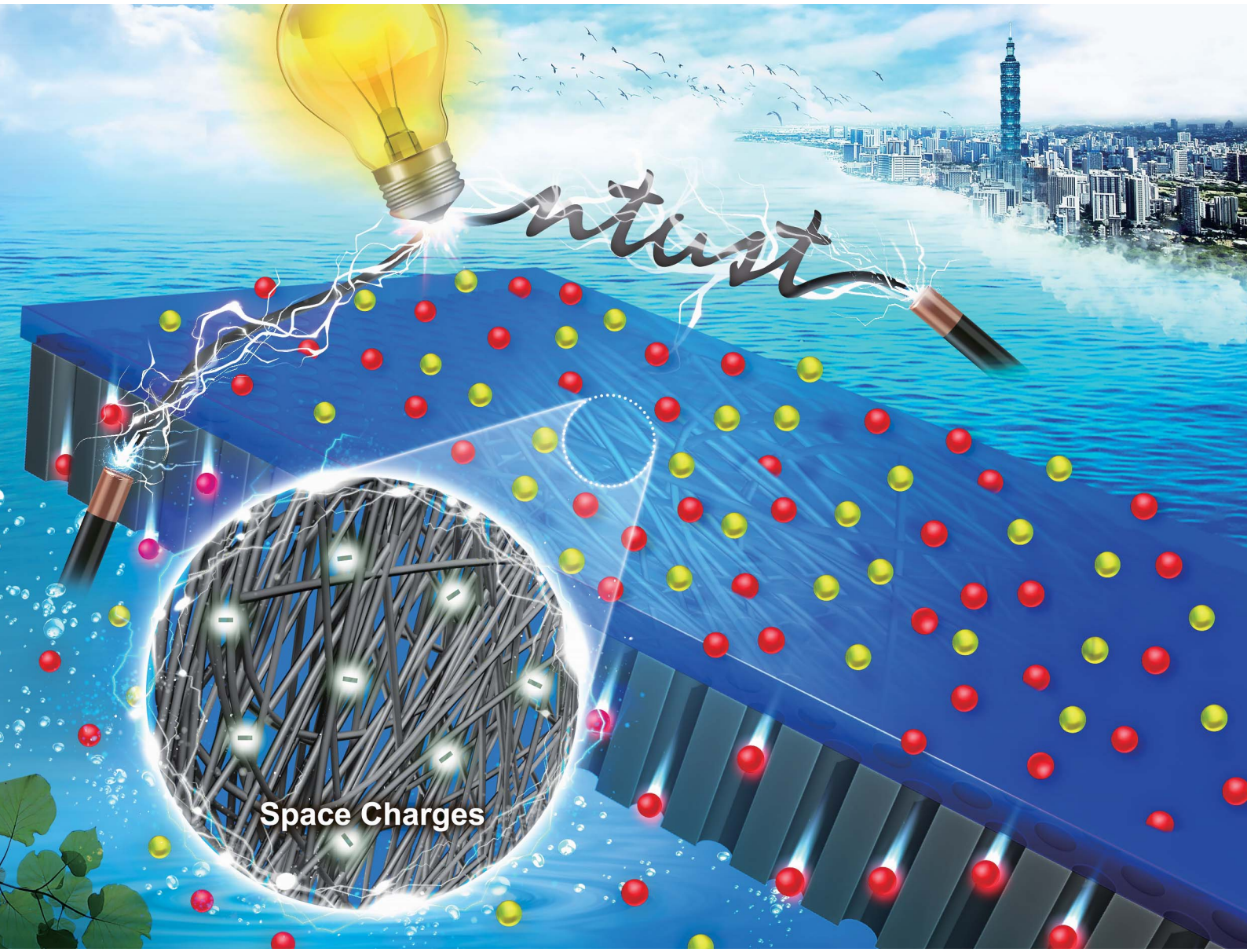

ISSN 2050-7488

ROYAL SOCIETY OF CHEMISTRY

PAPER

Li-Hsien Yeh *et al.*

Space charge enhanced ion transport in heterogeneous polyelectrolyte/alumina nanochannel membranes for high-performance osmotic energy conversion

Published on 10 December 2021. Downloaded by National Taiwan University of Science and Technology on 2/8/2022 4:55:38 PM.

Journal of Materials Chemistry A

ROYAL SOCIETY OF CHEMISTRY

PAPER

View Article Online
View Journal | View Issue

Check for updates

Cite this: *J. Mater. Chem. A*, 2022, **10**, 2867

Space charge enhanced ion transport in heterogeneous polyelectrolyte/alumina nanochannel membranes for high-performance osmotic energy conversion†

Chen-Wei Chang,‡ Chien-Wei Chu,‡ Yen-Shao Su‡ and Li-Hsien Yeh *

Osmotic energy captured from a salinity gradient *via* an ion-selective membrane is regarded as one of the renewable clean energy resources to meet the increasing global energy demands. However, due to insufficient ion selectivity and high resistance, the output power achieved by most of the existing membranes is still below the commercial benchmark (5 W m^{-2}), which restricts their practical applications. Herein, we report a simple drop-casting method for the fabrication of a polyelectrolyte (PE)-based heterogeneous ionic diode membrane consisting of a highly ordered alumina nanochannel membrane (ANM) and a space-charged Nafion layer. As demonstrated by experimental investigations and theoretical simulations, the incorporation of a space-charged PE layer into the heterogeneous membrane induces apparent ion rectification as well as shows enhanced ion transport and selectivity, which largely boost the osmotic energy conversion efficiency. When synthetic seawater and river water are mixed, the developed PE-based ionic diode membrane can achieve an osmotic power density as high as 5.13 W m^{-2}. This output power can be further upgraded to 22.1 W m^{-2} by mixing synthetic salt lake water and river water (5 M/0.01 M NaCl gradient), surpassing the performance of all the state-of-the-art ion-selective membranes. This work provides significant insights into the use of space-charged PE materials for the exploration of high osmotic energy harvesters.

Received 3rd October 2021
Accepted 6th December 2021

DOI: 10.1039/d1ta08560c

rsc.li/materials-a

Introduction

Developing renewable energies such as solar energy, wind power, and hydropower is an inevitable mission in the world because of the rocketing energy demands and air pollution issues resulting from the traditional power generation techniques.[1] Among the existing renewable energies, osmotic energy collecting chemical potential energy stored in a salinity gradient[2–4] has been regarded as a promising clean energy candidate owing to the naturally abundant resources such as seawater/river water interfaces. To effectively capture this kind of energy, a reverse electrodialysis (RED)-based technique is viewed as a promising technology that can directly convert chemical potential difference in the salinity gradient into electricity.[5–8] In conventional nanofluidic RED devices, the osmotic energy conversion was achieved using ion-selective membranes with homogeneous pore/channel materials.[9–13] However, suffering from unsatisfactory ion selectivity, limited ionic flux, and/or high internal resistance, the output power densities from most of the RED-based ion-selective membranes are still far below the commercial benchmark (5 W m^{-2}), restricting the practical applications.

Ion current rectification (ICR) is a unique diode-like ion transport property,[14–16] which can be observed in nanofluidics with asymmetric properties such as pore sizes, geometries, charges, and wettabilities, and allows preferential and enhanced ion transport.[17] The rectified pores have been demonstrated to improve RED-based osmotic energy conversion.[18–20] Thus, several heterogeneous membranes with ICR property (or called ionic diode membranes) have been reported for energy harvesting from salinity gradients.[21–31] Although many reports have shown improved ion transport and/or selectivity stemming from the ionic-diode effect, the improvement of output power was still limited because of the increased membrane resistance from heterogeneous pore materials.[23,24] Reducing the membrane thickness can assist in maximizing the power output,[30,31] but the fabrication of ultrathin heterogeneous membranes requires to be carried out *via* complicated and multi-step processes, which hampers their future industrial applications. Consequently, developing a facile method that can be used to fabricate the heterogeneous ionic diode membrane with enhanced ion transport and selectivity as well

Department of Chemical Engineering, National Taiwan University of Science and Technology, Taipei 10607, Taiwan. E-mail: lhyeh@mail.ntust.edu.tw; Tel: +886-2-27376942

† Electronic supplementary information (ESI) available. See DOI: 10.1039/d1ta08560c

‡ These authors contributed equally to this work.

Published on 10 December 2021. Downloaded by National Taiwan University of Science and Technology on 2/8/2022 4:55:38 PM.

as decreased resistance is an urgent requirement for improved energy conversion from salinity gradients.

In this study, we report a strategy combining a cation-selective Nafion PE layer and a highly ordered ANM to facilely fabricate a heterogeneous ionic diode membrane (Nafion/ANM) by a simple drop-casting method for improved osmotic energy conversion. The former bearing ample negatively charged sulfonate groups is able to render the heterogeneous membrane locally space-charged for enhanced cation selectivity,[32] and the latter composed of numerous straight and connected nanochannels can facilitate ion transport and then reduce membrane resistance. It is expected that the combination of the negatively space-charged Nafion and the positively surface-charged ANM[35,36] can create asymmetric charge distribution in the designed heterogeneous membrane, inducing a diode-like ICR property.[14] The experimental and simulation results show that the asymmetric design of the heterogeneous Nafion/ANM with a highly space-charged property can contribute to excellent ion selectivity, enhanced ion transport and apparent ICR effect, shedding light on improved osmotic energy conversion. When synthetic seawater (0.5 M NaCl) and river water (0.01 M NaCl) are mixed through the developed heterogeneous membrane, an output power density as high as 5.13 W m^{-2} is reached, exceeding the commercial benchmark. Notably, the power density can be further amplified to an unprecedentedly high value up to ~22.1 W m^{-2} by mixing synthetic salt lake water and river water (500-fold NaCl gradient), surpassing the reported values from all the state-of-the-art membranes under the same testing conditions. We believe that the PE-incorporated ionic diode membrane system presented can offer a promising platform for the development of highly efficient osmotic energy generators and ultrafast transport ionic devices.

Results and discussion

Fabrication of Nafion/ANM

Fig. 1a depicts the fabrication of the heterogeneous nanochannel membrane Nafion/ANM, consisting of a layer of Nafion and an ANM substrate with numerous highly ordered straight nanochannel arrays. To fabricate the heterogeneous membrane, the Nafion solution was first drop-casted on the top of the ANM, which was prepared *via* a two-step anodization procedure[33] (Fig. S1, ESI†), followed by thermal annealing at 45 °C for one day (see details in Experimental section). It is expected that in a mild neutral aqueous solution, the Nafion behaves like a highly space-charged polyelectrolyte (PE) layer due to the existence of abundant negatively charged sulfonate groups in the Nafion polymer matrix[34] and the ANM bears positive surface charges originating from protonated alumina functional groups on the channel walls,[35,36] creating an asymmetric charge distribution in the designed heterogeneous membrane (Fig. 1a). The chemical structure of Nafion was confirmed by the Fourier transform infrared (FTIR) spectroscopy (Fig. S2, ESI†), revealing the obvious signals (*i.e.*, 1058 and 1135 cm^{-1}) from sulfonate groups.[37] The morphologies of the Nafion/ANM were characterized by scanning electron microscopy (SEM), revealing that the surface of the Nafion layer was smooth and without obvious cracks or phase-separated pore structures, and the pore size and pore density of ANM were ~52 nm and ~3.3 × 10^{10} pores per cm^2, respectively (Fig. 1b and S3a, ESI†). The cross-sectional SEM view of the membrane illustrated in Fig. 1c indicates the distinct two-layer structures, comprising a dense Nafion PE layer (~4.1 μm) and a highly ordered nanochannel array layer (~38.8 μm). Contact angle measurements on both the Nafion and ANM sides of Nafion/ANM indicate that the heterogeneous membrane was slightly

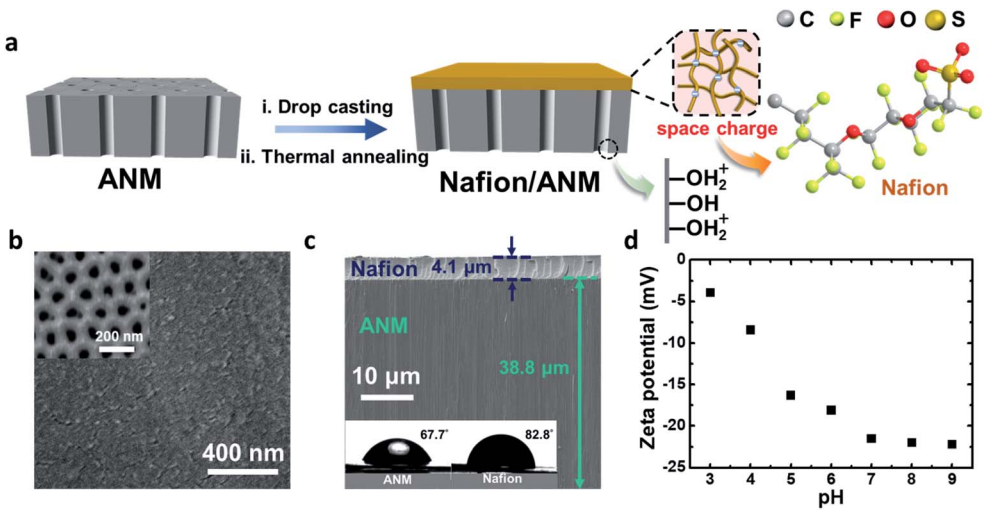

Fig. 1 Fabrication and characterization of Nafion/ANM. (a) Scheme depicting the fabrication process of the heterogeneous nanochannel membrane, Nafion/ANM. The Nafion PE layer is negatively space-charged and the ANM carries positive surface charges. (b) Nafion-side SEM image of the Nafion/ANM. The inset is the corresponding SEM image obtained at the ANM side. The pore size of ANM is ~52 nm. (c) Cross-sectional SEM image of the Nafion/ANM. The thicknesses of the Nafion and ANM layers are about 4.1 μm and 38.8 μm, respectively. The insets depict the contact angle results on the ANM (left) and Nafion (right) surfaces of the heterogeneous membrane, respectively. (d) Dependence of pH on the membrane zeta potential of Nafion at 10 mM KCl.

 This journal is © The Royal Society of Chemistry 2022

Published on 10 December 2021. Downloaded by National Taiwan University of Science and Technology on 2/8/2022 4:55:38 PM.

with hydrophilicity and asymmetric wettabilities (insets in Fig. 1c). The membrane zeta potential measurements of the Nafion show that it indeed carries negative charges and the charge nature is independent of the solution pH (Fig. 1d). The strong cation selectivity of the negatively charged Nafion layer was proven by energy-dispersive X-ray spectroscopy (EDX) mappings, exhibiting a much stronger intensity of potassium than chlorine captured after immersing the membrane in 1 M KCl solution for 30 min (Fig. S3b, ESI†). We expected that the space-charge property of the Nafion used can remarkably enhance the membrane ion selectivity,[38,39] and the creation of the membrane asymmetry in charges, geometries and wettabilities in the Nafion/ANM is able to realize rectification of ion transport, which has been proven with the potential in promoting osmotic energy conversion efficiency through amplified ionic current.[18–20]

Space charge-enhanced ion transport and selectivity

The ion transport properties of the Nafion/ANM were investigated by measuring the current–voltage (*I–V*) curves under various testing conditions using a homemade conductive cell (see details in Experimental section). As the first step, we tested the ICR ability of the heterogeneous membranes, where KCl was adopted as the testing electrolyte because of similar diffusivities of the two major transporting ions, K^+ and Cl^- ($\sim 2 \times 10^{-9}$ m^2 s^{-1}).[40,41] As expected, compared with the homogeneous ANM and Nafion membranes revealing the linear *I–V* responses (ohmic behavior), the heterogeneous Nafion/ANM shows apparent non-linear ICR effect (diode-like behavior)[42,43] with a ratio of 15.6 (Fig. 2a and S4, ESI†). For all the concentrations tested, the current and conductance at positive voltages are higher than those at negative voltages of the same magnitude, indicating that the Nafion/ANM can rectify ion transport even in high-concentration 500 mM KCl solutions (Fig. 2a and S5, ESI†). The rectification ability of the ionic diode membrane can be quantified by estimating the ICR ratio defined as the ratio of currents at +2 V and −2 V.[44] The averaged rectification abilities of the Nafion/ANM made were about 15.1-, 18.2-, 10.3- and 2.0-times in 1 mM, 10 mM, 100 mM and 500 mM KCl solutions (Fig. 2b and Table S1, ESI†). The local maximum dependence of rectification ability on the salt concentration is consistent with the previous experimental findings[45–47] and theoretical predictions[48,49] for various types of nanofluidic didoes. This dependence could be attributed to the net effects of the Debye length screening and amount of enriched/depleted ions at the nanoconfinement.[50] In addition, we tested the ANM thickness effect on the rectification ability of Nafion/ANM (Fig. 2c and Table S2, ESI†). It is pointed out that a relatively higher ICR ratio (>10-fold) can be reached using the ANM with a relatively low thickness (<62.2 μm). It is expected that a thinner nanochannel membrane reveals a smaller ion transportation resistance,[35] which might lead to an increase in rectification if this effect dominates the ion transport behavior. It is

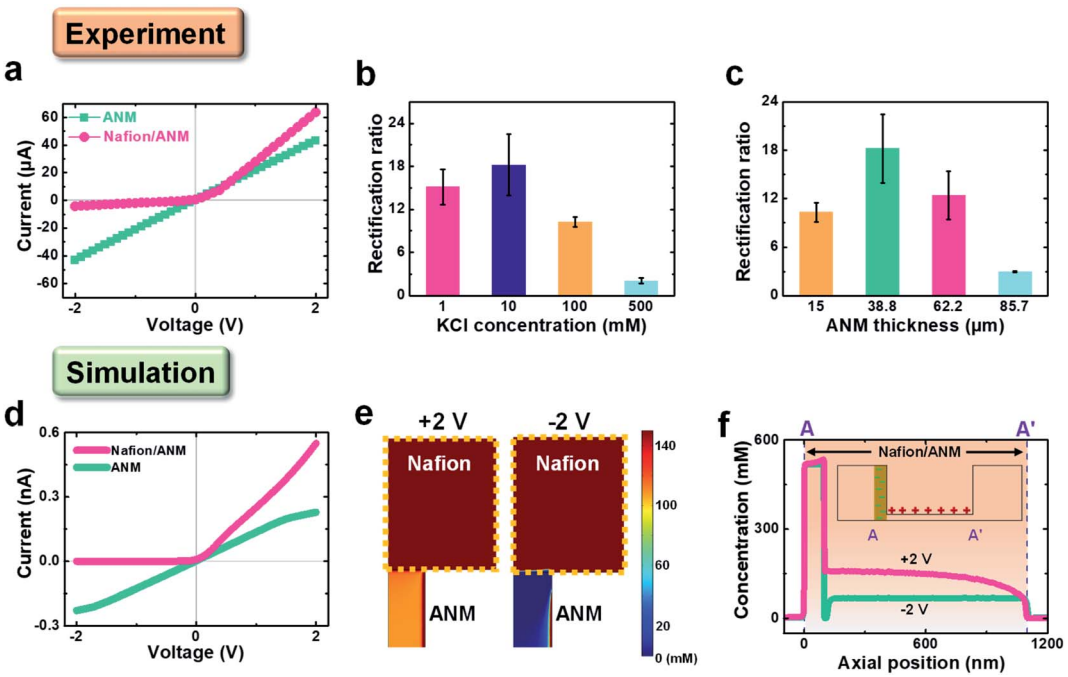

Fig. 2 Space charge-regulated ion transport in the Nafion/ANM. (a–c) Experimental and (d–f) simulated ion transport behaviors of the Nafion/ANM system considered. (a) Experimental *I–V* curves of the Nafion/ANM and the pure ANM substrate recorded in 1 mM KCl solution. Summarized ICR ratios as a function of the (b) KCl concentration and (c) ANM thickness. The salt concentration in (b) is fixed at 10 mM. (d) Simulated *I–V* curves of the Nafion/ANM and ANM in 1 mM KCl. In the simulation, we assumed that the space charge density of the Nafion layer is -5×10^7 C m^{-3} and the surface charge density on the ANM wall is 0.08 C m^{-2}. (e) Spatial variations in the total ionic concentration in the region focusing on the interface of the Nafion/ANM at a transmembrane voltage of +2 V (left) and −2 V (right). The dotted curve highlights the Nafion region with a space charge. Enrichment and depletion of ions in the Nafion/ANM can be found at +2 V and −2 V, respectively. (f) Axial variations of the total ionic concentration in the Nafion/ANM.

Published on 10 December 2021. Downloaded by National Taiwan University of Science and Technology on 2/8/2022 4:55:38 PM.

noted that although the decrease in the ANM thickness decreases ion transportation resistance and thus increases rectification ability, it can also reduce the total positive surface charges on the ANM walls. The latter effect would mitigate the asymmetric degree of charge distribution in the heterogeneous Nafion/ANM, and if this effect dominates, the rectification ability of Nafion/ANM may start to decrease with the decrease in the ANM thickness (Fig. 2c). Similar behaviors can be found in Fig. S6 (ESI),† where the rectification ratio of Nafion/ANM decreases from ~18.2 to ~4, as the Nafion thickness increases from ~4.1 μm to ~35.3 μm, attributed to the increase in ion transportation resistance. We also tested the influence of the pore size of the ANM on the rectification ability of Nafion/ANM in 10 mM KCl solution (Fig. S7, ESI†). The ICR ratios of Nafion/ANM with the ANM pore diameters of ~27, ~52 and ~92 nm measured were about 9.2, 18.2 and 3.2, respectively, suggesting that an ionic diode membrane with higher rectification efficiency can be realized using the ANM with a smaller pore size. We therefore confirmed that the incorporation of a space-charged Nafion PE layer into the considered heterogeneous membrane can create the asymmetries of charges and geometries,[14,15,51] inducing significant diode-like ICR effects.

To clearly understand the underlying physics behind the rectification of Nafion/ANM, we modeled the current–voltage curve of the system comprising a space-charged Nafion PE layer and a cylindrical nanochannel (Fig. S8, ESI†) based on the modified Poisson–Nernst–Planck and Stokes–Brinkman equations (see details in Experimental section and ESI†). As shown in Fig. 2d, the simulated *I–V* curves of the Nafion/ANM and ANM systems considered are in excellent agreement with the experimental findings (Fig. 2a). The former rectifies ion current and shows preferential and enhanced ion transport at positive voltages, but the latter does not rectify and shows voltage-independent *I–V* response. The rectification of the Nafion/ANM is supported by the voltage-dependent variations in total ionic concentration (Fig. 2e and f), which show the enrichment (depletion) of ions near the region of ANM close to the Nafion and ANM interface at +2 V (−2 V). However, the simulated symmetric ANM shows the expected voltage-independent variations in total ionic concentration (Fig. S9, ESI†).

As the second step, we investigated the osmotic ion transport of the Nafion/ANM by analyzing its *I–V* characteristics under a series of NaCl concentration gradients (Fig. 3). In the experimental setup, we fixed the low concentration at 0.01 M in the reservoir adjacent to the ANM side and changed the high concentration from 0.5 M to 5 M in the other side reservoir (Fig. 3a). The choice of this design stems from the fact that the amplified open-circuit voltage (V_{oc}) and closed-circuit current (I_{sc}) could improve the ion selectivity and transportation under this salinity gradient direction (Fig. S10, ESI†). Fig. 3b illustrates the *I–V* curves recorded by applying a 0.5 M/0.01 M NaCl gradient through the Nafion/ANM and ANM systems. As shown, the former can produce a V_{oc} of ~121 mV and an I_{sc} of ~4.84 μA,

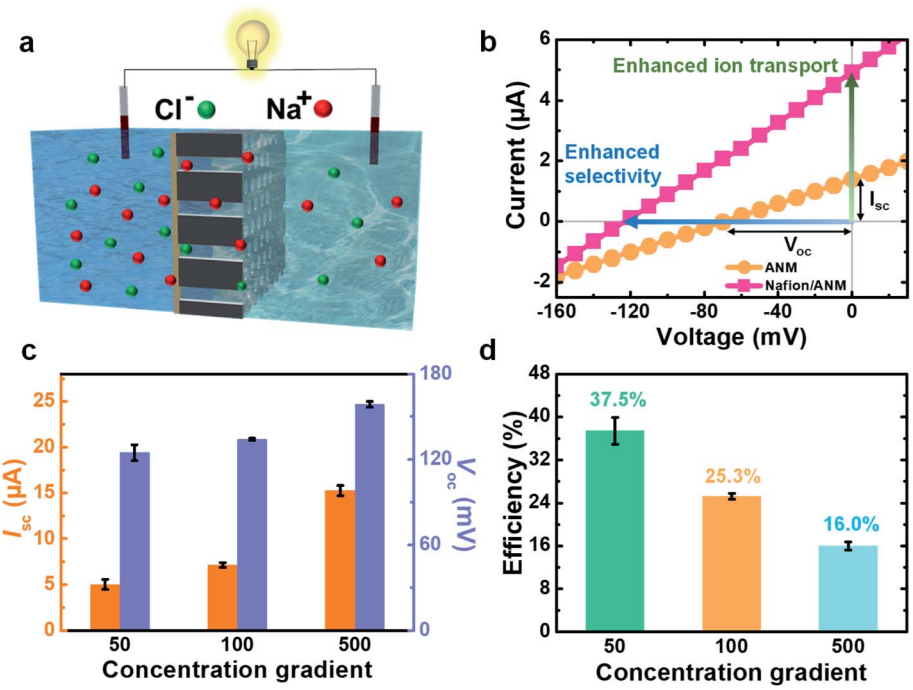

Fig. 3 Space charge-enhanced osmotic energy conversion. (a) Schematic of the osmotic energy conversion device used, where the Nafion side of the heterogeneous membrane is in contact with a higher concentration solution. (b) *I–V* curves of the Nafion/ANM and ANM recorded in the 0.5 M/0.01 M NaCl concentration gradient. The open-circuit voltage (V_{oc}) and closed-circuit current (I_{sc}) of the ANM are *ca.* 69.5 mV and 1.39 μA, respectively, and both the corresponding values are enhanced up to 121 mV and 4.84 μA for the Nafion/ANM. The remarkable amplification of V_{oc} and I_{sc} indicates the enhanced ion selectivity and ion transport with the incorporation of a space-charged Nafion PE layer. (c) Achieved I_{sc}, V_{oc} and (d) energy conversion efficiency of Nafion/ANM as a function of the NaCl gradient. The low concentration is fixed at 0.01 M.

 This journal is © The Royal Society of Chemistry 2022

Published on 10 December 2021. Downloaded by National Taiwan University of Science and Technology on 2/8/2022 4:55:38 PM.

both of which are remarkably larger than those outputted from the ANM (V_{oc} of ~69.5 mV and I_{sc} of ~1.39 μA). Introduction of a highly space-charged Nafion PE layer onto the ANM increases V_{oc} and I_{sc} by approximately 74.1% and 248%, respectively. This proves the space charge enhanced ion selectivity and ion transportation in Nafion/ANM. We then estimated the salt concentration gradient-dependent osmotic energy conversion performance (Fig. 3c, d, and Table S3, ESI†). It should be noted that to estimate the pure concentration gradient-driven performance (*e.g.*, osmotic potential, V_{osm}, and maximum energy conversion efficiency, η_{max}), the electrode calibration with the redox potential, resulting from the uneven potential drop at the electrodes in the presence of a concentration gradient, has been performed (see Fig. S11 and details in the ESI†).[21] As expected, both I_{sc} and V_{oc} increase with the increase in the NaCl concentration gradient (Fig. 3c), due to the increase in the driving force for osmotic transport.[52] Moreover, the produced V_{osm} are all higher than 75 mV regardless of the levels of concentration gradient, resulting in a high cation selectivity ($t^+ > 0.783$) of the heterogeneous membrane (Table S3 and Fig. S12, ESI†). Consequently, the Nafion/ANM can achieve conversion efficiencies of *ca.* 37.5, 25.3 and 16.0% at 50-, 100- and 500-fold NaCl gradients, respectively (Fig. 3d and Table S3, ESI†). It should be noted that by mixing synthetic seawater and river water (0.5 M/0.01 M NaCl gradient), the averaged efficiency realized by the heterogeneous Nafion/ANM can be as high as 37.5%, reaching the high-performance level compared with the other state-of-the-art ion-selective membranes reported (Table S4, ESI†). The superior efficiency of the heterogeneous membrane could be attributed to the significantly enhanced cation selectivity.

Ultrahigh osmotic power in high saline environments

The results shown in Fig. 2 and 3 indicate that the incorporation of a highly space-charged Nafion PE layer into the heterogeneous membrane is capable of inducing apparent ICR effects and significantly improving the membrane ion selectivity and ion transport. This suggests the potential use of the Nafion/ANM as a high-efficiency osmotic power generator. To demonstrate this, we then tested the practical osmotic power output by transferring the generated current (I) from the measured system to an external load resistor with a tunable resistance of R_L and the power was calculated as $P = I^2 \times R_L$.[21,25] Fig. 4a shows that regardless of the salinity gradient, the output current density decreases with the increase in external resistance and drops sharply when the external resistance approaches the internal resistance of the membrane, in agreement with the earlier reports.[21,25] Consequently, the power density goes through a local maximum with the increase in external resistance and the maximum output power density can be identified as R_L equal to the internal resistance of the membrane (Fig. 4b). The Nafion/ANM can achieve the maximum osmotic power densities as

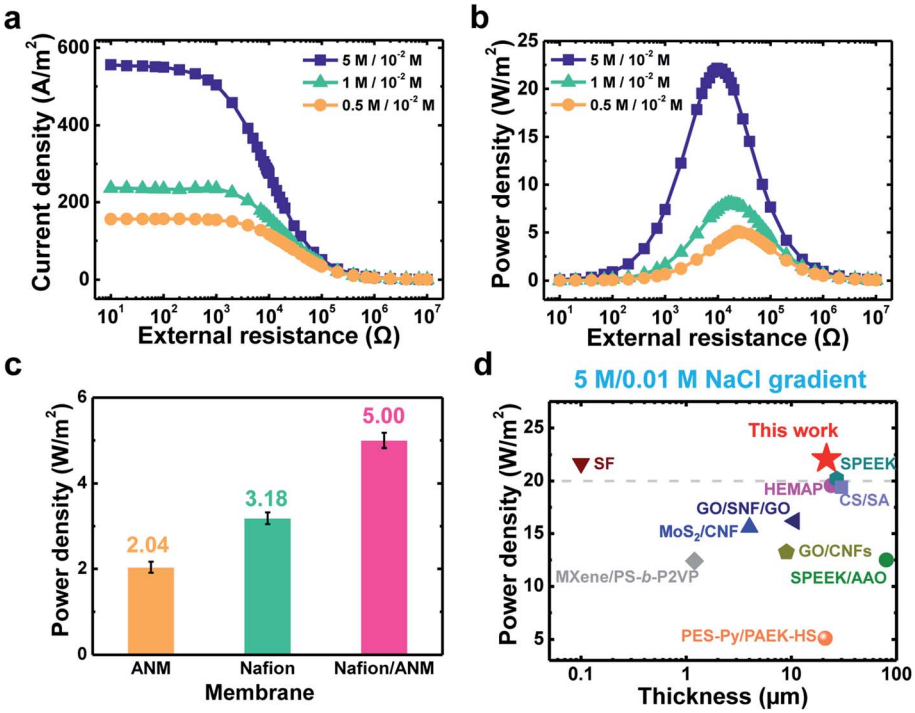

Fig. 4 Ultrahigh osmotic power generation in a hypersaline environment. (a) Generated current density and (b) power density of the Nafion/ANM as a function of the external load resistance at different NaCl gradients. The maximum power densities achieved are 5.13, 8.08 and 22.1 W m^{-2} at 50-fold, 100-fold and 500-fold concentration gradients, respectively. (c) Power density output achieved by the ANM, Nafion, and Nafion/ANM at a 50-fold NaCl gradient. (d) Comparison of the osmotic power densities achieved by the Nafion/ANM and the reported ion-selective membranes at the same 5 M/0.01 M NaCl gradient.

Published on 10 December 2021. Downloaded by National Taiwan University of Science and Technology on 2/8/2022 4:55:38 PM.

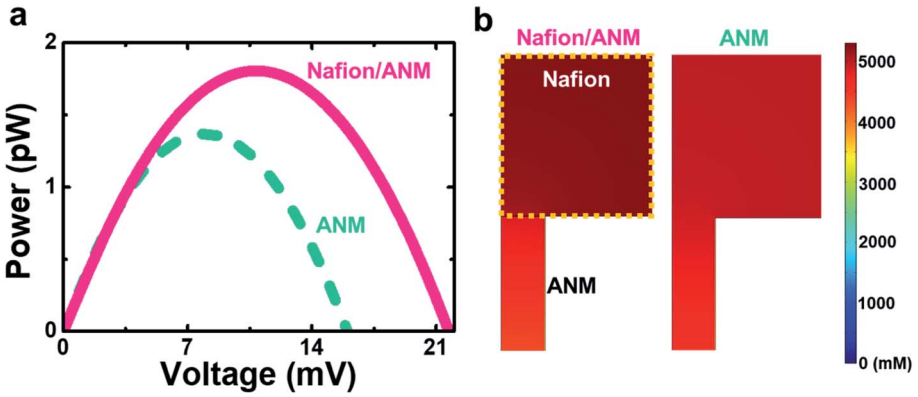

Fig. 5 Theoretical demonstration of the space charge-enhanced osmotic power. Simulated (a) *P*–*V* curves and (b) contours of the counterion concentration in the Nafion/ANM and ANM systems under consideration at a 500-fold salinity gradient.

high as about 5.13, 8.08 and 22.1 W m^{-2} at the resistances of 24, 16 and 9.8 kΩ under the 50-fold, 100-fold and 500-fold NaCl gradients, respectively (Fig. 4b and S13, ESI†). The increase in the salinity gradient leads to an increase in the osmotic power and a decrease in the membrane resistance, in agreement with the results of previous works.[21,26] Notably, when synthetic seawater and river water (0.5 M/0.01 M NaCl gradient) are mixed, the maximum power density produced by the Nafion/ANM is up to 5.13 W m^{-2}, which crosses the commercial benchmark (5 W m^{-2}) and surpasses that of most of the previously reported nanochannel membranes[21–27,53–56] (Table S4, ESI†).

We also compared the osmotic power generated from the heterogeneous Nafion/ANM with that of the pure Nafion membrane and ANM, which show nearly 57% and 145% improvements, respectively, under the same testing condition (Fig. 4c and S14, ESI†). This proves the space charge-enhanced osmotic power by incorporation of a Nafion PE layer into a heterogeneous ionic diode membrane. The influences of the Nafion thickness and the AMN pore size were further investigated in a 0.5 M/0.01 M NaCl gradient for a deeper understanding of the optimal conditions for the heterogeneous membrane design (Fig. S15, ESI†). As shown, the increase in the Nafion thickness from 4.1 μm to 35.3 μm leads to a decrease in the averaged power density from 5.00 W m^{-2} to 1.01 W m^{-2} (Fig. S15c, ESI†), attributed to the increase in the ion transportation resistance. In addition, the outputted power density of the Nafion/ANM can be maximized by using the ANM with a pore diameter of ~52 nm (Fig. S15f, ESI†). Similar behaviors can be found in Fig. S7,† where the Nafion/ANM shows the highest rectification ability by using the ANM with a pore diameter of ~52 nm. It shows that the ionic diode membrane with a higher ionic rectification ability is able to produce a higher osmotic power.

It should be noted that we also compared the output power density from the Nafion/ANM with that of all the earlier reported state-of-the-art ion-selective membranes under the condition where salt lake water (5 M NaCl) is mixed with river water (0.01 M NaCl),[23,28,39,55–60] as shown in Fig. 4d and Table S5 (ESI).† Most surprisingly, under such high saline conditions, the power density achieved reaches an unprecedentedly high value (22.1 W m^{-2}), as compared to earlier works (Fig. 4d). From the above-demonstrated facts, it can be inferred that the significant improvement in the osmotic energy conversion performance (especially in hypersaline environments) could be attributed to the space charge-enhanced ion transport and selectivity as well as the rectification effect.

To support the space charge-enhanced osmotic power, we modeled the two power–voltage curves based on the Nafion/ANM and ANM systems considered. The system parameters used in the simulations are the same as those in Fig. 2d, and the details of the model can be found in our previous works[20,61] and in the ESI.† The simulation results shown in Fig. 5a indicate that the considered Nafion/ANM system indeed can achieve a higher maximum osmotic power than that of the ANM, in agreement with the experimental finding. The boosting osmotic power can also be supported by the higher selectivity to counterions by the Nafion/ANM, as shown in Fig. 5b. We also tested the salinity gradient direction effect on the osmotic power conversion of the space-charged system under consideration (Fig. S16, ESI†). Consistent with our experimental finding, the space-charged Nafion side of the Nafion/ANM in contact with a higher concentration solution can achieve a higher osmotic power. This finding is inconsistent with the earlier study,[41] which considered the Nafion layer as a local apparent surface charge and reported that a better efficiency can be realized by setting a lower concentration solution in the Nafion side. All the experimental and simulation results shown above feature the essential role that the space-charged PE layer plays in the enhancement of current rectification and osmotic energy conversion in the heterostructured membrane.

Conclusions

In summary, we have demonstrated that the incorporation of a space-charged PE Nafion layer into a heterogeneous membrane can reveal significant ionic rectification even under high salt conditions and amplify ion transport and selectivity, thus achieving high osmotic energy harvesting. By mixing synthetic seawater and river water (0.5 M/0.01 M NaCl gradient), the exploited PE-based ionic diode membrane can deliver

 This journal is © The Royal Society of Chemistry 2022

Published on 10 December 2021. Downloaded by National Taiwan University of Science and Technology on 2/8/2022 4:55:38 PM.

a power density of about 5.13 W m^{-2}, across the commercial benchmark. Most importantly, the power density achieved can be boosted up to ~22.1 W m^{-2} in hypersaline environments (5 M/0.01 M NaCl gradient), which is the highest among all the reported osmotic energy generators. All the experimental findings of the diode-like ion transport property and boosted osmotic power are well supported by our simulations, which provide insights into the underlying mechanism of space-charge enhanced properties. This study not only provides fundamental basis but also opens up a new avenue of using PE materials for high energy harvesting from salty solutions.

Experimental section

Fabrication of the Nafion/ANM

The main ANM substrates with highly ordered straight channels were fabricated by a two-step anodization method (Fig. S1, ESI†) as described earlier.[25,35] The as-received aluminum foils (Al, 99.9995%) were electropolished with a mixed $HClO_4$ (20 vol%) and ethanol (80 vol%) solution under 20 V at room temperature for 90 s. The polished Al foils were first anodized by 0.3 M $H_2C_2O_4$ solution at 20 °C under 50 V for 30 min and then all the disordered oxidized layers were removed by the mixed CrO_3 (1.8 wt%) and H_3PO_4 (6 wt%) solution at 60 °C for 1 h. Then, the treated Al foils were anodized second time under the same condition of the first anodization for 1, 3, 5, and 8 h to receive membranes with different lengths of the alumina nanochannel array. To receive the ANMs with connected pores, the remaining Al layers were removed by a mixed $CuCl_2$ (1.5 wt%) and HCl (53 wt%) solution at room temperature, followed by the removal of the residual barrier layers by 5 wt% H_3PO_4 at 30 °C for 70 min. The heterogeneous nanochannel membrane Nafion/ANM was fabricated by drop-casting 10 μL of 5% Nafion 117 solution (Sigma-Aldrich) onto the as-prepared ANM, followed by a thermal annealing process in an oven at 45 °C for 24 h.

Material characterizations

The morphological and elemental characterizations of the Nafion/ANM were performed using a scanning electron microscope (SEM; JSM-7900F, JEOL) equipped with an EDX detector at an accelerating voltage of 10 kV. The contact angle measurements were conducted by dropping a 5 μL pure water droplet on each side of Nafion/ANM surfaces using a goniometer equipped with an optical surface analyzer (OSA60-G, Ningbo NB Scientific Instruments). The membrane zeta potentials of the Nafion film were characterized using a zeta potential analyzer (SurPASS 3, Anton Paar) in 10 mM KCl solutions at different pH values. The FTIR spectrum of the Nafion pressed in KBr pellets was recorded using a spectrometer (Trace-100, Shimadzu) in the range of 400–4000 cm^{-1}.

Electrical measurement

The ion transport property and osmotic energy conversion performance of all the devices used were tested using a Keithley 6487 picoammeter (Keithley Instruments, Cleveland, Ohio) through a custom-made conductive cell and a pair of Ag/AgCl electrodes. The fabricated membranes were mounted between two half-compartments of the conductive cell. For ion transport property tests, the current–voltage (I–V) curves were recorded with KCl solutions of different designed concentrations. For osmotic energy conversion tests, the working electrode was placed in a higher-concentration compartment and three sets of NaCl concentration gradients (50-fold, 100-fold, and 5000-fold) were adopted. For fair comparison, all measurements of the output current density and power density were carried out with an effective testing area of ~3×10^4 μm^2, the same as that used in the previously reported studies.[22,23,25]

Multiphysics simulation

All current–voltage (I–V) curves of the PE/nanochannel system under consideration in the absence and presence of a salinity gradient were simulated by simultaneously solving the modified Poisson–Nernst–Planck and Stokes–Brinkman equations,[62] which have been proven to be accurate in capturing the underlying physics of ion transport property in similar PE-based nanofluidic systems.[16,63–65] To receive an affordable computational cost, we simplified the Nafion as a PE layer bearing a uniformly distributed space charge density of -5×10^7 C m^{-3}, in accordance with the typical values of synthetic polyelectrolytes (*ca.* 1×10^6–1×10^8 C m^{-3}),[66,67] and the ANM as a cylindrical channel of 25 nm radius and 1000 nm length. We assumed that the ANM carries a surface charge density of 0.08 C m^{-2}, in agreement with previous studies.[61,68] The other details of the governing equations, boundary conditions and parameters used in the simulation can be found in the ESI.† The model adopted was numerically solved using the commercial finite element software, COMSOL Multiphysics 4.3a, on a high-performance computer.

Author contributions

Chen-Wei Chang: methodology, formal analysis, investigation, data curation, visualization, validation, investigation, writing – original draft. Chien-Wei Chu: formal analysis, investigation, writing – original draft, writing – review & editing. Yen-Shao Su: software, formal analysis, investigation, visualization, validation, investigation. Li-Hsien Yeh: conceptualization, methodology, writing – original draft, writing – review & editing, supervision, project administration, funding acquisition.

Conflicts of interest

There are no conflicts to declare.

Acknowledgements

This work was financially supported by the Ministry of Science and Technology (MOST), Taiwan under Grants MOST 108-2628-E-011-006-MY3, 108-2221-E-011-103-MY3, 108-2638-E-002-003-MY2 (Shackleton Program award), 110-2223-E-011-003-MY3, and 110-2124-M-002-013-.

Published on 10 December 2021. Downloaded by National Taiwan University of Science and Technology on 2/8/2022 4:55:38 PM.

Notes and references

1 S. Chu and A. Majumdar, *Nature*, 2012, **488**, 294–303.
2 A. Siria, M. L. Bocquet and L. Bocquet, *Nat. Rev. Chem.*, 2017, **1**, 0091.
3 M. Macha, S. Marion, V. V. R. Nandigana and A. Radenovic, *Nat. Rev. Mater.*, 2019, **4**, 588–605.
4 Z. Zhang, L. P. Wen and L. Jiang, *Nat. Rev. Mater.*, 2021, **6**, 622–639.
5 A. Siria, P. Poncharal, A. L. Biance, R. Fulcrand, X. Blase, S. T. Purcell and L. Bocquet, *Nature*, 2013, **494**, 455–458.
6 J. D. Feng, M. Graf, K. Liu, D. Ovchinnikov, D. Dumcenco, M. Heiranian, V. Nandigana, N. R. Aluru, A. Kis and A. Radenovic, *Nature*, 2016, **536**, 197–200.
7 X. Liu, M. He, D. Calvani, H. Y. Qi, K. Gupta, H. J. M. de Groot, G. J. A. Sevink, F. Buda, U. Kaiser and G. F. Schneider, *Nat. Nanotechnol.*, 2020, **15**, 307–312.
8 Z. H. Lin, W. S. Hsu, A. Preet, L. H. Yeh, Y. H. Chen, Y. P. Pao, S. F. Lin, S. Lee, J. C. Fan, L. Wang, Y. P. Chiu, B. S. Yip and T. E. Lin, *Nano Energy*, 2021, **79**, 105440.
9 J. Hwang, S. Kataoka, A. Endo and H. Daiguji, *Lab Chip*, 2016, **16**, 3824–3832.
10 S. Hong, F. W. Ming, Y. Shi, R. Y. Li, I. S. Kim, C. Y. Y. Tang, H. N. Alshareef and P. Wang, *ACS Nano*, 2019, **13**, 8917–8925.
11 L. H. Yeh, Z. Y. Huang, Y. C. Liu, M. J. Deng, T. H. Chou, H. C. O. Yang, T. Ahamad, S. M. Alshehri and K. C. W. Wu, *J. Mater. Chem. A*, 2019, **7**, 26791–26796.
12 P. Liu, Y. Sun, C. C. Zhu, B. Niu, X. D. Huang, X. Y. Kong, L. Jiang and L. P. Wen, *Nano Lett.*, 2020, **20**, 3593–3601.
13 V. P. Mai and R. J. Yang, *Appl. Energy*, 2020, **274**, 115294.
14 Z. S. Siwy, *Adv. Funct. Mater.*, 2006, **16**, 735–746.
15 Y. Ai, M. K. Zhang, S. W. Joo, M. A. Cheney and S. Qian, *J. Phys. Chem. C*, 2010, **114**, 3883–3890.
16 Z. Zeng, Y. Ai and S. Qian, *Phys. Chem. Chem. Phys.*, 2014, **16**, 2465–2474.
17 Z. Zhang, L. P. Wen and L. Jiang, *Chem. Soc. Rev.*, 2018, **47**, 322–356.
18 J. P. Hsu, T. C. Su, P. H. Peng, S. C. Hsu, M. J. Zheng and L. H. Yeh, *ACS Nano*, 2019, **13**, 13374–13381.
19 M. Y. Gao, P. C. Tsai, Y. S. Su, P. H. Peng and L. H. Yeh, *Small*, 2020, **16**, 2006013.
20 P. C. Tsai, Y. S. Su, M. Gao and L. H. Yeh, *J. Mater. Chem. A*, 2021, **9**, 20502–20509.
21 J. Gao, W. Guo, D. Feng, H. T. Wang, D. Y. Zhao and L. Jiang, *J. Am. Chem. Soc.*, 2014, **136**, 12265–12272.
22 W. W. Xin, Z. Zhang, X. D. Huang, Y. H. Hu, T. Zhou, C. C. Zhu, X. Y. Kong, L. Jiang and L. P. Wen, *Nat. Commun.*, 2019, **10**, 3876.
23 X. B. Zhu, J. R. Hao, B. Bao, Y. H. Zhou, H. B. Zhang, J. H. Pang, Z. H. Jiang and L. Jiang, *Sci. Adv.*, 2018, **4**, eaau1665.
24 S. H. Hou, Q. R. Zhang, Z. Zhang, X. Y. Kong, B. Z. Lu, L. P. Wen and L. Jiang, *Nano Energy*, 2021, **79**, 105509.
25 Y. C. Liu, L. H. Yeh, M. J. Zheng and K. C. W. Wu, *Sci. Adv.*, 2021, **7**, eabe9924.
26 X. Sui, Z. Zhang, C. Li, L. C. Gao, Y. Zhao, L. J. Yang, L. P. Wen and L. Jiang, *ACS Appl. Mater. Interfaces*, 2019, **11**, 23815–23821.
27 R. R. Li, J. Q. Jiang, Q. Q. Liu, Z. Q. Xie and J. Zhai, *Nano Energy*, 2018, **53**, 643–649.
28 X. Lin, P. Liu, W. Xin, Y. Teng, J. Chen, Y. Wu, Y. Zhao, X. Y. Kong, L. Jiang and L. P. Wen, *Adv. Funct. Mater.*, 2021, **31**, 2105013.
29 T. L. Xiao, J. Ma, Z. Y. Liu, B. X. Lu, J. Q. Jiang, X. Y. Nie, R. F. Luo, J. Jin, Q. Q. Liu, W. P. Li and J. Zhai, *J. Mater. Chem. A*, 2020, **8**, 11275–11281.
30 K. X. Chen, L. N. Yao and B. Su, *J. Am. Chem. Soc.*, 2019, **141**, 8608–8615.
31 Z. Zhang, X. Sui, P. Li, G. H. Xie, X. Y. Kong, K. Xiao, L. C. Gao, L. P. Wen and L. Jiang, *J. Am. Chem. Soc.*, 2017, **139**, 8905–8914.
32 T. J. Ma, E. Balanzat, J. M. Janot and S. Balme, *ACS Appl. Mater. Interfaces*, 2019, **11**, 12578–12585.
33 C. W. Chu, Y. C. Huang, C. C. Tsai and J. T. Chen, *Eur. Polym. J.*, 2015, **63**, 141–148.
34 S. T. Cui, J. W. Liu, M. E. Selvan, D. J. Keffer, B. J. Edwards and W. V. Steele, *J. Phys. Chem. B*, 2007, **111**, 2208–2218.
35 Y. S. Su, S. C. Hsu, P. H. Peng, J. Y. Yang, M. Y. Gao and L. H. Yeh, *Nano Energy*, 2021, **84**, 105930.
36 C. Y. Li, F. X. Ma, Z. Q. Wu, H. L. Gao, W. T. Shao, K. Wang and X. H. Xia, *Adv. Funct. Mater.*, 2013, **23**, 3836–3844.
37 A. Gruger, A. Regis, T. Schmatko and P. Colomban, *Vib. Spectrosc.*, 2001, **26**, 215–225.
38 W. P. Chen, Q. R. Zhang, Y. C. Qian, W. W. Xin, D. Z. Hao, X. L. Zhao, C. C. Zhu, X. Y. Kong, B. Z. Lu, L. Jiang and L. P. Wen, *ACS Cent. Sci.*, 2020, **6**, 2097–2104.
39 W. P. Chen, Q. Wang, J. J. Chen, Q. R. Zhang, X. L. Zhao, Y. C. Qian, C. C. Zhu, L. S. Yang, Y. Y. Zhao, X. Y. Kong, B. Z. Lu, L. Jiang and L. P. Wen, *Nano Lett.*, 2020, **20**, 5705–5713.
40 L. Mei, L. H. Yeh and S. Qian, *Nano Energy*, 2017, **32**, 374–381.
41 Y. D. Wu, Y. C. Qian, B. Niu, J. J. Chen, X. F. He, L. S. Yang, X. Y. Kong, Y. F. Zhao, X. B. Lin, T. Zhou, L. Jiang and L. P. Wen, *Small*, 2021, **17**, 2101099.
42 I. Vlassiouk and Z. S. Siwy, *Nano Lett.*, 2007, **7**, 552–556.
43 T. J. Ma, J. M. Janot and S. Balme, *Small Methods*, 2020, **4**, 2000366.
44 C. Y. Lin, L. H. Yeh and Z. S. Siwy, *J. Phys. Chem. Lett.*, 2018, **9**, 393–398.
45 D. Zhang, S. Q. Zhou, Y. Liu, X. Fan, M. L. Zhang, J. Zhai and L. Jiang, *ACS Nano*, 2018, **12**, 11169–11177.
46 C. Zhao, H. C. Zhang, J. Hou, R. W. Ou, Y. L. Zhu, X. Y. Li, L. Jiang and H. T. Wang, *ACS Appl. Mater. Interfaces*, 2020, **12**, 28915–28922.
47 C. Wang, F. F. Liu, Z. Tan, Y. M. Chen, W. C. Hu and X. H. Xia, *Adv. Funct. Mater.*, 2020, **30**, 1908804.
48 S. J. Tseng, S. C. Lin, C. Y. Lin and J. P. Hsu, *J. Phys. Chem. C*, 2016, **120**, 25620–25627.
49 J. P. Hsu, Y. M. Chen, S. T. Yang, C. Y. Lin and S. Tseng, *J. Colloid Interface Sci.*, 2018, **531**, 483–492.
50 L. J. Cheng and L. J. Guo, *Chem. Soc. Rev.*, 2010, **39**, 923–938.

 This journal is © The Royal Society of Chemistry 2022

Published on 10 December 2021. Downloaded by National Taiwan University of Science and Technology on 2/8/2022 4:55:38 PM.

51 T. W. Lin, J. P. Hsu, C. Y. Lin and S. Tseng, *J. Phys. Chem. C*, 2019, **123**, 12437–12443.
52 S. Tseng, Y. M. Li, C. Y. Lin and J. P. Hsu, *Nanoscale*, 2016, **8**, 2350–2357.
53 Z. Zhang, S. Yang, P. P. Zhang, J. Zhang, G. B. Chen and X. L. Feng, *Nat. Commun.*, 2019, **10**, 2920.
54 L. Cao, H. Wu, C. Y. Fan, Z. M. Zhang, B. B. Shi, P. F. Yang, M. Qiu, N. A. Khan and Z. Y. Jiang, *J. Mater. Chem. A*, 2021, **9**, 14576–14581.
55 W. W. Xin, H. Y. Xiao, X. Y. Kong, J. J. Chen, L. S. Yang, B. Niu, Y. C. Qian, Y. F. Teng, L. Jiang and L. P. Wen, *ACS Nano*, 2020, **14**, 9701–9710.
56 C. C. Zhu, P. Liu, B. Niu, Y. N. Liu, W. W. Xin, W. P. Chen, X. Y. Kong, Z. Zhang, L. Jiang and L. P. Wen, *J. Am. Chem. Soc.*, 2021, **143**, 1932–1940.
57 Y. D. Wu, W. W. Xin, X. Y. Kong, J. J. Chen, Y. C. Qian, Y. Sun, X. L. Zhao, W. P. Chen, L. Jiang and L. P. Wen, *Mater. Horiz.*, 2020, **7**, 2702–2709.
58 Y. Y. Zhao, J. Wang, X. Y. Kong, W. W. Xin, T. Zhou, Y. C. Qian, L. S. Yang, J. H. Pang, L. Jiang and L. P. Wen, *Natl. Sci. Rev.*, 2020, **7**, 1349–1359.
59 G. S. Bian, N. Pan, Z. H. Luan, X. Sui, W. X. Fan, Y. Z. Xia, K. Y. Sui and L. Jiang, *Angew. Chem., Int. Ed.*, 2021, **60**, 20294–20300.
60 J. J. Chen, W. W. Xin, X. Y. Kong, Y. C. Qian, X. L. Zhao, W. P. Chen, Y. Sun, Y. D. Wu, L. Jian and L. P. Wen, *ACS Energy Lett.*, 2020, **5**, 742–748.
61 L. H. Yeh, F. Chen, Y. T. Chiou and Y. S. Su, *Small*, 2017, **13**, 1702691.
62 D. C. Zheng and L. H. Yeh, *Micromachines*, 2020, **11**, 949.
63 L. H. Yeh, M. Zhang, S. Qian, J. P. Hsu and S. Tseng, *J. Phys. Chem. C*, 2012, **116**, 8672–8677.
64 C. Y. Lin, J. P. Hsu and L. H. Yeh, *Sens. Actuators, B*, 2018, **258**, 1223–1229.
65 W. C. Huang and J. P. Hsu, *J. Colloid Interface Sci.*, 2019, **557**, 683–690.
66 Y. D. Wu, T. Zhou, Y. Wang, Y. C. Qian, W. P. Chen, C. C. Zhu, B. Niu, X. Y. Kong, Y. F. Zhao, X. B. Lin, L. Jiang and L. P. Wen, *Nano Energy*, 2022, **92**, 106709.
67 Z. Zeng, L. H. Yeh, M. Zhang and S. Qian, *Nanoscale*, 2015, **7**, 17020–17029.
68 Z. Zhang, X. Y. Kong, K. Xiao, G. H. Xie, Q. Liu, Y. Tian, H. C. Zhang, J. Ma, L. P. Wen and L. Jiang, *Adv. Mater.*, 2016, **28**, 144–150.